# Mapping Carrier Diffusion in Single Silicon Core−Shell Nanowires with Ultrafast Optical Microscopy

M. A. Seo,* J. Yoo, S. A. Dayeh, S. T. Picraux, A. J. Taylor, and R. P. Prasankumar*

Center for Integrated Nanotechnologies, Los Alamos National Laboratory, Los Alamos, New Mexico 87545, United States

ABSTRACT: Recent success in the fabrication of axial and radial core−shell heterostructures, composed of one or more layers with different properties, on semiconductor nanowires (NWs) has enabled greater control of NW-based device operation for various applications.[1−3] However, further progress toward significant performance enhancements in a given application is hindered by the limited knowledge of carrier dynamics in these structures. In particular, the strong influence of interfaces between different layers in NWs on transport makes it especially important to understand carrier dynamics in these quasi-one-dimensional systems. Here, we use ultrafast optical microscopy[4] to directly examine carrier relaxation and diffusion in single silicon core-only and Si/SiO$_2$ core−shell NWs with high temporal and spatial resolution in a noncontact manner. This enables us to reveal strong coherent phonon oscillations and experimentally map electron and hole diffusion currents in individual semiconductor NWs for the first time.

KEYWORDS: Ultrafast spectroscopy, semiconductor nanowires, optical properties, carrier diffusion, carrier relaxation
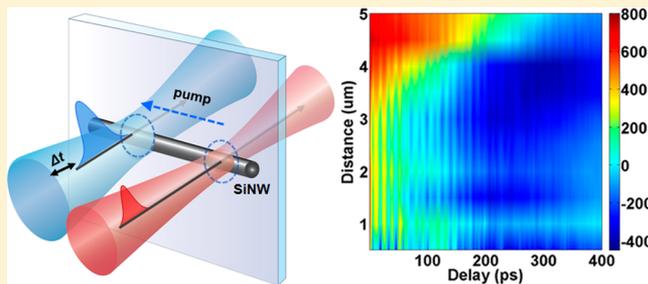
Controlled synthesis of semiconductor nanowires (NWs) has greatly extended NW functionality into a variety of applications such as NW-based energy harvesting systems,[5] tunnel FETs,[6] and light-emitting diodes (LEDs).[7,8] Often, a core/shell structure is desired for tailoring energy band-edge profiles to control charge transport and improve device performance, exemplified by the investigation of Si NW arrays with axial and radial p−n junctions for photovoltaic applications.[5,9,10] To achieve competitive device performance, it is important to study charge transport mechanisms and the speed of charge separation along the length of a semiconductor NW as well as the influence of a core−shell interface on these processes. Although several recent studies have described the experimental characterization of these processes in both bulk semiconductors[11] and semiconductor nanostructures[12] with simultaneously high spatial and temporal resolution, to date no spatiotemporal plots of diffusion currents for either electrons or holes have ever been experimentally constructed in any semiconductor material.

Here, we report the first experimental mapping of diffusion currents in a semiconductor NW. Our technique relies on the use of ultrafast optical microscopy (UOM) to track charge carrier transport through space and time in single silicon NWs.[4] While earlier UOM experiments have studied carrier dynamics at fixed positions along a semiconductor NW,[4,13−15] we have probed carrier concentration gradients dynamically along the length of the NW, which enabled us to construct separate diffusion current maps for electrons and holes. The basic principle behind our technique is as follows: when a strong optical "pump" pulse injects carriers into a semiconductor nanowire, the photoexcited carriers are initially in a non-equilibrium state,[16] which creates a carrier density gradient along the nanowire. Since there is no external electric field across the NW in our experimental configuration, diffusion takes place due to the variation in concentration of the carriers along the NW axis, which results in associated internal fields.[17] The carrier density at a given position is then detected by a weaker "probe" pulse as a function of time delay and spatial separation between the two pulses, allowing one to extract the carrier flow (diffusion current) along the NW axis. This is possible since, under typical experimental conditions, the measured photoinduced change in transmission, $\Delta T/T$, is directly proportional to the carrier density within the probe spot.[16,18] Therefore, by measuring the $\Delta T/T$ signal at a specific position and varying the pump position along the NW axis, we can both measure carrier relaxation at a given position and map the carrier diffusion current along the NW at ultrashort time scales.

In our experiments, a striking difference was observed in carrier relaxation and diffusion for Si NWs with or without a high-quality SiO$_2$ shell layer, as the SiO$_2$ layer passivates surface states and therefore minimizes carrier trapping. Effectively, this allowed us to experimentally show how shell passivation influences carrier concentration gradients and improves the efficacy of electron and hole diffusion currents in nanoscale semiconductor channels. Furthermore, our UOM measurements clearly revealed strong acoustic phonon oscillations in both Si and Si/SiO$_2$ NWs, which have not been previously reported, to the best of our knowledge, and indicate the

excellent structural integrity of our material system. These new observations cannot be probed by conventional contact-based methods for studying minority carrier transport in semiconductor systems such as scanning photocurrent microscopy (SPCM) or electron-beam-induced current (EBIC) analysis,[9,19] and as such these are the first spatiotemporal measurements of diffusion currents and phonon oscillations in single Si NWs.

Our UOM system and a conceptual illustration of UOM with spatially separated pump and probe beams are shown in Figures 1a and 1b, respectively (see Methods section). The Si NWs
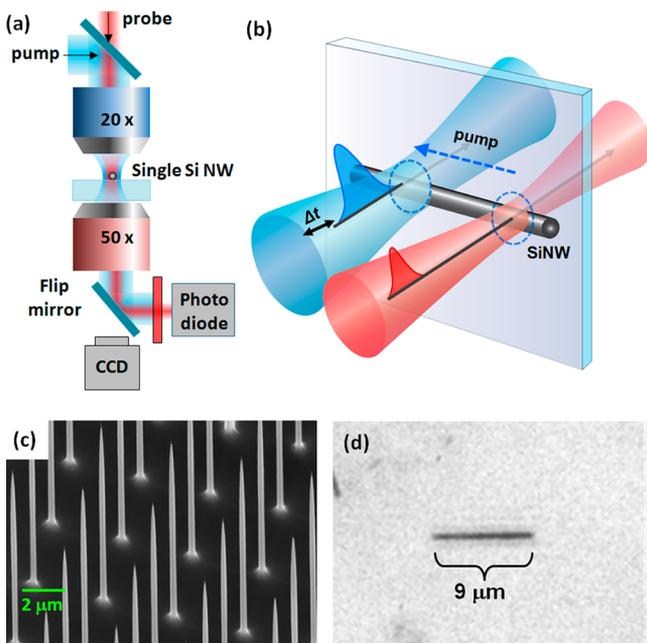

Figure 1. Ultrafast optical microscopy system. (a) Experimental setup for ultrafast optical microscopy on single nanowires. (b) A conceptual illustration of UOM with spatially separated pump and probe beams. The blue arrow depicts the direction in which the pump beam is moved along the NW axis. (c) SEM image of pillar-type Si NWs on the silicon substrate. (d) Optical microscope image of a single Si NW on a sapphire substrate, taken in our UOM system.

were fabricated by a combination of e-beam lithography and Si deep reactive ion etching, followed by thermal oxidation and stripping steps to form pristine NW surfaces (Figure 1c) and transferred onto a transparent sapphire substrate, as shown in the image taken in our UOM system (Figure 1d). To assess the

material quality of our NWs and provide reference measurements, we first overlap our pump and probe spots and measure photoinduced transmission changes at one end of two single core-only Si NWs with diameters of $d = 167$ nm and $d = 255$ nm as well as a $d = 255$ nm single Si/SiO$_2$ core−shell NW (where d refers to the core diameter throughout this paper) (Figure 2a). The measured transmission changes can be fit with two decay time constants; here, we focus on the longer time constant τ that is due to carrier diffusion, trapping, and recombination, since the fast time constant is due to electron−phonon relaxation[20] and does not change significantly with the addition of a SiO$_2$ shell. In addition, note that the signals for both core-only NWs have small negative values at long time delays. This is due to induced absorption that occurs after carriers are trapped into midgap surface states,[21] supported by the fact that no negative signal is observed in Figure 2a for the core−shell NW, in which these surface states are passivated. Finally, we note that carrier diffusion away from the initial excitation point also influences the observed dynamics at longer time scales, which will be discussed in more detail below.

The magnitude of the $\Delta T/T$ signal from the core−shell Si NW is about twice that of the bare Si NW, and the decay time τ is faster in the bare Si NW (∼90 ps for the 167 nm Si NW and ∼121 ps for the 255 nm Si NW) than in the 255 nm core−shell NW (∼211 ps) owing to the surface passivation provided by the SiO$_2$ shell. These values are somewhat longer than those previously measured on vapor−liquid−solid (VLS) grown Si NWs,[4] presumably due to the absence of a metal (Au) growth seed in our NWs, which results in NWs with a higher degree of crystallinity than typical NWs prepared with VLS approaches. Using the procedure for extracting the surface recombination velocity (SRV) described in refs 19 and 22, we find that Si core-only NWs have SRVs of 3.2×10^4 and 3.0×10^4 cm/s for 167 and 255 nm diameters and 8.2×10^3 cm/s for the Si/SiO$_2$ NW with 255 nm core diameter. The extracted SRVs from these NWs quantitatively compare well to previously measured values[4,20] and confirm that unpassivated (bare) NWs have higher surface recombination velocities than passivated (core−shell) NWs.

The enhanced structural integrity of our material system (due to the precision etching-based, top-down fabrication technique used here as compared to VLS growth) also enables us to uncover phononic properties of our NWs. Figure 2a reveals that the photoinduced transmission changes in all Si NWs measured here are accompanied by strong oscillations. Figure 2b depicts the Fourier transform of the oscillatory part
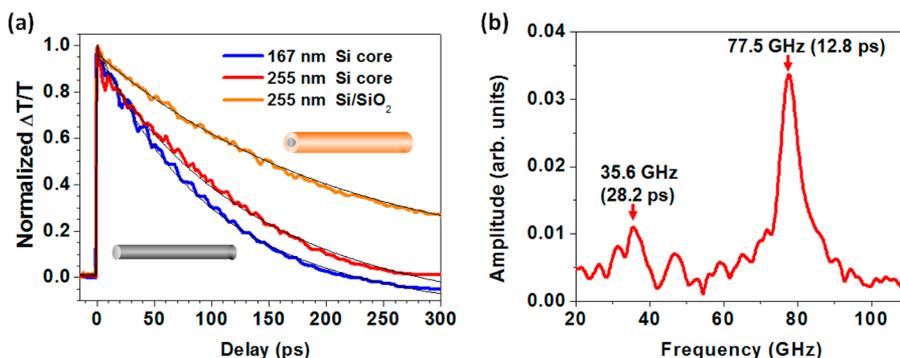

Figure 2. Photoinduced transmission changes in single Si NWs. (a) Normalized transmission changes ($\Delta T/T$) for overlapping pump and probe spots on single core-only Si NWs and a single SiO$_2$ encapsulated Si NW. Black lines show the double-exponential curve fits. (b) Fourier transform of the oscillatory component in the $\Delta T/T$ signal for the 255 nm Si core-only NW from (a).

of the $\Delta T/T$ signal from the 255 nm core-only Si NW in Figure 2a, revealing peaks at 35.6 and 77.5 GHz. These oscillations are typically attributed to coherent acoustic phonons, which were first observed by Thomsen et al. in 1984.[23] More recently, there have been reports on coherent phonons in single CdTe NWs[14] detected using ultrafast pump−probe spectroscopy as well as acoustic oscillations in InAs NW ensembles measured in time-resolved X-ray experiments.[24] The oscillations observed in both of those NW systems were attributed to localized breathing modes, in which the oscillation frequency is inversely proportional to the NW diameter. However, we find that the main 77.5 GHz peak in our data varies little with NW diameter (~79 GHz for the 167 nm core-only NW in Figure 2b and ~74.5 GHz for a ~450 nm core-only NW (not shown)). Instead, we attribute this peak to Brillouin oscillations.[23] Physically, when the pump pulse irradiates the NWs, it generates a longitudinal sound wave directed toward the sapphire substrate (normal to the NW axis), which then diffracts the time-delayed probe pulse when it enters the sample, causing strong oscillations in the intensity of the transmitted probe. The Brillouin oscillation period τ_B can be expressed by $\tau_B = \lambda/2n\nu$,[25] where the longitudinal sound velocity for bulk Si is $\nu = 9.32 \times 10^3$ m/s[26] and the refractive index is $n = 3.65$, giving a oscillation period $\tau_B = 12.5$ ps that is independent of the NW diameter; this agrees well with the measured value of 12.8 ps (Figure 2b). Because this acoustic oscillation is initiated by the photoexcited carriers in the Si core, the oscillation periods are the same for all Si NWs, with or without the SiO_2 layer. The weaker 35.6 GHz peak, in contrast, is attributed to excitation of the fundamental breathing mode, for which the model of ref 14 yields a predicted value of 34 GHz, in good agreement with our observations; this mode was observed both in this 255 nm NW as well as in the other two NW diameters mentioned above. Importantly, this demonstrates the coexistence of propagating strain waves and localized phonon modes in our NWs; a more detailed analysis will be the subject of a future publication. Finally, we note that no periodic oscillations were observed in the VLS-grown Si NWs used in previous experiments,[4] likely because the tapered shape of these NWs would cause the oscillations to quickly dephase and superpose destructively along the length of a given NW.[27]

While the measurements discussed above extend our understanding of the electronic and phononic properties of semiconductor NWs, the most striking features in our measurements arise when we spatially vary the location of our pump and probe spots. UOM experiments were conducted on a single Si NW (255 nm) and a single Si/SiO$_2$ NW (255 nm core and 75 nm thick shell) with the probe beam fixed near one end of the NW and the spatial separation between the pump and probe beams, l, varied to a maximum of 5 μm along the NW axis. It is important to note that our single Si NWs have very small diameter variation along their axis (<10 nm) throughout the bulk of the NW where our measurements were performed, making them excellent quasi-1D systems to investigate carrier diffusion along the NW axis. Figures 3a and 3b summarize spatiotemporal $\Delta T/T$ signals measured on the core-only and core/shell NWs. The rise time increases with l for both the bare Si NW and the Si/SiO$_2$ NW, revealing strong acoustic phonon oscillations in both cases. Interestingly, the maximum $\Delta T/T$ signal for the Si/SiO$_2$ NW stays nearly constant up to 4 μm but rapidly decreases as a function of l for the bare Si NW. This drastic decrease in $\Delta T/T$ for the bare Si NW is caused by carrier trapping and recombination occurring
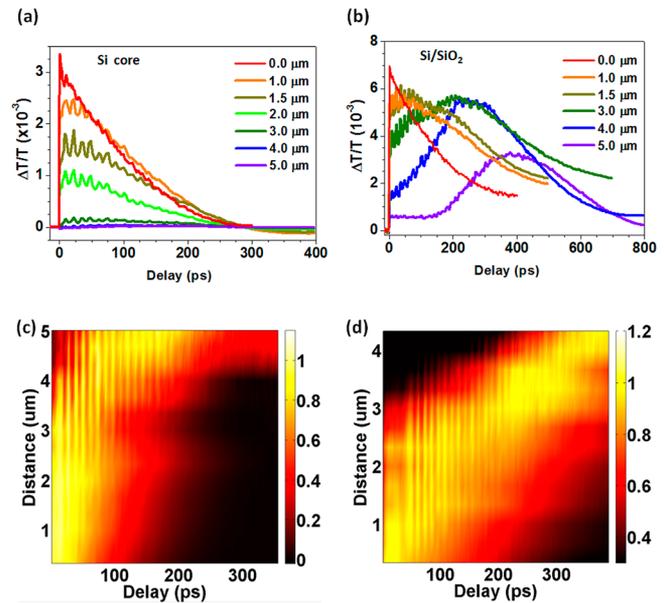

Figure 3. Mapping carrier dynamics in 255 nm diameter Si NWs. Photoinduced transmission changes for various pump−probe separations for (a) the bare Si NW and (b) the 75 nm SiO$_2$ shell encapsulated Si NW. Two-dimensional maps of the normalized $\Delta T/T$ signals as functions of separation and time delay are also shown for both NWs in (c) and (d).

at the surface of the NW.[16,28−31] In contrast, the SiO$_2$ layer in core/shell NWs reduces surface trapping and recombination as described above, enabling us to directly track carriers as they diffuse from one end to the other in a single semiconductor NW. The dramatic differences in time- and space-dependent carrier dynamics between the two NWs can be visualized in Figures 3c and 3d, which show contour plots of the normalized $\Delta T/T$ signal as a function of pump−probe separation and time delay.

To construct spatiotemporal diffusion current maps in our NWs, we first extract position-dependent carrier distributions for the Si core-only NW (Figure 4a) and the Si/SiO$_2$ core−shell NW (Figure 4b) from the contour plots in Figures 3c and 3d before normalization. Then, from the shape of the carrier distribution as a function of position at a specific time, we can directly obtain the diffusion coefficients for both NWs using a method based on the Haynes−Shockley experiment.[17] Specifically, we can calculate the average diffusion coefficient for electrons and holes, D_{avr}, using

$$D_{avr} = \frac{(\Delta x)^2}{16 t_d} \tag{1}$$

where Δx is the width of the carrier distribution (calculated by fitting with a Gaussian function) at a certain time, t_d. This relation is only valid without drift and when neglecting recombination, so we measured Δx for $t_d < \tau$ for each NW (85 ps for the Si core-only NW and 115 ps for the Si/SiO$_2$ NW). The extracted diffusion coefficients are 35 cm^2/s for the Si core-only NW and 53 cm^2/s for the Si/SiO$_2$ NW, which are somewhat larger than but still comparable to the values for bulk Si.[32]

When the pump signal photoexcites a carrier density at one position in a NW (Δn_{pump}^{tot}), the probe measures a carrier density greater than that at equilibrium (Δn_{pump}^{tot}), and in the absence of an applied external field, the photoexcited carriers
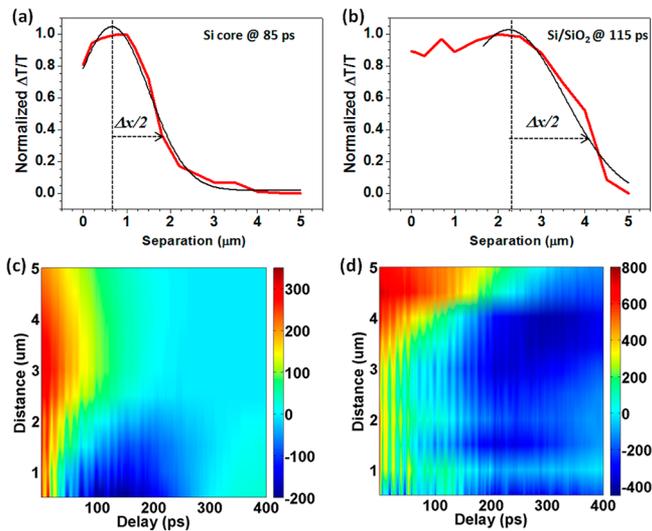
Figure 4. Mapping diffusion currents in Si NWs. Position-dependent carrier distribution along the NWs at specific times for (a) a Si core-only NW and (b) a Si/SiO$_2$ NW. Two-dimensional diffusion current maps for (c) the core-only NW and (d) the core–shell NW, respectively. Note that in our color scheme, red denotes positive values of the diffusion current, while blue denotes negative values. In addition, please note that we derived (c) and (d) from Figures 3a and 3b, not Figures 3c and 3d, since the data in Figures 3c and 3d are normalized and would therefore lead to inaccurate values of $J(x,t)$.

will diffuse from the pump position (x_{pump}) to the probe position (x_{probe}) (defined as the $+x$ direction). Since the measured $\Delta T/T$ signal is proportional to the carrier density under these conditions,[16,18] the total diffusion current, J, can then be expressed as[17]

$$J_{total}(x, t) = J_n(x, t) + J_p(x, t)$$

$$\approx qD \frac{\Delta n_{pump}^{tot} - \Delta n_{probe}^{tot}}{x_{pump} - x_{probe}}$$

$$\propto qD \frac{\Delta T/T_{overlap} - \Delta T/T_{separation}}{x_{pump} - x_{probe}} \qquad (2)$$

This includes both electron ($J_n(x,t) = -qD[\partial n(x,t)/\partial x]$) and hole ($J_p(x,t) = qD[\partial p(x,t)/\partial x]$) contributions, which will always be positive for electrons and negative for holes under our experimental conditions. This difference in the sign of $J(x,t)$ for electrons and holes arises because the electrons diffuse in the $+x$ direction (causing $\partial n(x,t)/\partial x < 0$)) with a charge of $-q$, while holes will diffuse in the same direction (causing $\partial p(x,t)/\partial x < 0$) with a charge of $+q$. Therefore, when $J(x,t) > 0$, the diffusion current is dominated by electron transport, and when $J(x,t) < 0$, the diffusion current is dominated by hole transport. Importantly, this allows us to separate out the contributions of electrons and holes to the total diffusion current. It is worth noting that eqs 1 and 2 do not take into account local electric field and carrier lifetime variations that could be induced by the large carrier concentration gradients, which may affect the extracted values for the diffusion coefficients and currents. However, we find that the carrier lifetime does not significantly vary with position in either NW (e.g., for the core–shell NW τ = 211 ps for l = 0 μm and τ = 245 ps for l = 3 μm), and the extracted diffusion coefficients compare reasonably well to

those in bulk Si. This suggests that eqs 1 and 2 are a reasonable description of the observed phenomena.

Spatiotemporal maps of the diffusion current derived from the $\Delta T/T$ data in Figures 3a and 3b using eq 2 are depicted for both the bare Si NW (Figure 4c) and the core–shell NW (Figure 4d). For the bare Si NW, we can notice that electron diffusion currents evolve and decay over a relatively short time scale and throughout the entire length of the NW. This is due to the strong concentration gradient of electrons (Figure 3c) resulting from surface recombination throughout the entire NW length. For the core/shell NW, where the electron concentration is sustained throughout most of the NW length (Figure 3d), making the concentration gradients smaller, we find that electron diffusion currents are appreciable toward the far end of the NW away from the pump location and are as a consequence sustained for significantly longer times than for the bare Si NW. The relatively short-lived nature of the electron diffusion currents in both types of NWs corroborates with earlier studies showing that surface states in Si NWs are dominantly acceptor-type and trap electrons.[33]

In contrast, the heavier effective masses of holes cause a delay in the evolution of their diffusion currents. In addition, due to their lower diffusion coefficients, the magnitude of the hole diffusion current is observed to be lower than that of electrons. Consequently, for bare Si NWs, hole diffusion currents appear only over short distances from the probe spot, while many of the diffused electrons get trapped by surface states far away from the pump location. For the core/shell NWs, in the absence of strong recombination at the surface, a larger number of holes will propagate down the NW to recombine with the electrons that have traveled to the NW end away from the pump spot. Hole diffusion currents therefore will be sustained over longer distances in the core/shell NWs.

The experimental observation of both electron and hole diffusion currents in a semiconductor nanowire is uniquely attained by our measurement technique and captures some of the most basic principles of semiconductor physics in a simple and straightforward analysis; in fact, our results essentially correspond to a "textbook" case of carrier diffusion in a quasi-1D semiconductor after an impulse excitation.[17] Furthermore, our experiments enable us to extract several fundamental parameters in these NWs, including the surface recombination velocity, diffusion coefficients, and diffusion velocities, without the influence of contacts. The results presented here thus have implications for semiconductor devices in a wide variety of applications that use minority carriers as the main charge transport mechanism, such as in optoelectronics, bipolar transistors, and sensitive photodetectors.[1,34] Finally, the noncontact nature of ultrafast optical microscopy will enable us to directly observe the interactions of carriers with different interfaces within a single nanowire, making it particularly useful for future investigations of radial and axial NW hetero-structures, where charge transport across heterointerfaces is of particular interest for advanced device architectures (e.g., NW-based p–n junctions).

Methods. Our ultrafast optical microscopy setup is based on a femtosecond Ti:sapphire laser oscillator centered at 840 nm, the output of which is divided into pump and probe beams, with the probe power <10% of the pump power. The pump beam is then frequency-doubled in a BBO crystal to generate femtosecond pulses at 420 nm. By using a 20× (0.4 NA) microscopic objective lens, the pump (5 μm spot size) and probe (2 μm spot size) beams are collinearly focused at the

sample position, with polarization of both beams parallel to the NW axis. The pump fluence used here was 126.0 $\mu J/cm^2$, leading to an initial photoexcited carrier density of $n(0) = 5.9 \times 10^{19}$ cm^{-3}, according to the calculation method used in previous work.[4] By slightly tilting the pump beam angle, we can spatially separate the two beam spots, which enables us to directly track charge carriers along the NW axis (Figure 1b). The transmitted probe light was then collected through a 50× objective lens, and its intensity was measured by a photodiode, while the NW and light positions are simultaneously monitored using a CCD camera. Real time monitoring of the focused pump and probe spots allows us to control their positions on the NW. This setup allowed us to significantly improve the spatial resolution over our previous work[4,21] (Figure 1a).

The Si NWs were fabricated by a combination of e-beam lithography and Si deep reactive ion etching. After preparation of as-etched Si[111] NWs with an average diameter of 600 nm and an average length of 9 μm, the diameters were reduced to d = 167 and 255 nm by one or more thermal oxidation and subsequent SiO_2 wet etching steps (Figure 1c). Prepared bare Si NWs and Si/SiO_2 core−shell NWs with a 150 nm SiO_2 shell grown in a dry O_2 stream at 1000 °C were then dispersed on sapphire substrates by chemical dropping, where they lay flat on the surface (Figure 1d). A single NW out of the randomly dispersed NW ensemble was then chosen for our optical measurements. By looking at the back side of the samples with a 50× objective lens, variable zoom lens, and CCD camera, in that order, we can easily locate individual Si NWs. We performed the same experiments on at least three different NWs for each NW diameter, allowing us to confirm that the carrier dynamics and diffusion behavior are consistent for all cases.

■ AUTHOR INFORMATION

Corresponding Author
*E-mail: minahseo@lanl.gov (M.A.S.); rpprasan@lanl.gov (R.P.P.).

Notes
The authors declare no competing financial interest.

■ ACKNOWLEDGMENTS

■ REFERENCES

(1) Gudiksen, M. S.; Lauhon, L. J.; Wang, J.; Smith, D. C.; Lieber, C. M. *Nature* **2002**, *415* (6872), 617−620.

(2) Garnett, E. C.; Yang, P. *J. Am. Chem. Soc.* **2008**, *130* (29), 9224−9225.

(3) Tian, B.; Zheng, X.; Kempa, T. J.; Fang, Y.; Yu, N.; Yu, G.; Huang, J.; Lieber, C. M. *Nature* **2007**, *449* (7164), 885−889.

(4) Seo, M. A.; Dayeh, S. A.; Upadhya, P. C.; Martinez, J.; Swartzentruber, B. S.; Picraux, S. T.; Taylor, A. J.; Prasankumar, R. P. *Appl. Phys. Lett.* **2012**, *100*, 071104.

(5) Kelzenberg, M. D.; Boettcher, S. W.; Petykiewicz, J. A.; Turner-Evans, D. B.; Putnam, M. C.; Warren, E. L.; Spurgeon, J. M.; Briggs, R. M.; Lewis, N. S.; Atwater, H. A. *Nat. Mater.* **2010**, *9*, 239−244.

(6) Bjork, M. T.; Knoch, J.; Schmid, H.; Riel, H.; Riess, W. *Appl. Phys. Lett.* **2008**, *92* (19), 193504.

(7) Gudiksen, M. S.; Lauhon, L. J.; Wang, J.; Smith, D. C.; Lieber, C. M. *Nature* **2002**, *415*, 617−620.

(8) Yan, R.; Gargas, D.; Yang, P. D. *Nat. Photonics* **2009**, *3*, 569−576.

(9) Kelzenberg, M. D.; Turner-Evans, D. B.; Kayes, B. M.; Filler, M. A.; Putnam, M. C.; Lewis, N. S.; Atwater, H. A. *Nano Lett.* **2008**, *8* (2), 710−714.

(10) Picraux, S. T.; Yoo, J.; Campbell, I. H.; Dayeh, S. A.; Perea, D. E. *Semiconductor Nanowires for Solar Cells in Semiconductor Nanostructures for Optoelectronic Devices*; Springer: Berlin, 2012.

(11) Ruzicka, B. A.; Werake, L. K.; Samassekou, H.; Zhao, H. *Appl. Phys. Lett.* **2010**, *97* (26), 262119.

(12) Fickenscher, M. A.; Jackson, H. E.; Smith, L. M.; Yarrison-Rice, J. M.; Kang, J. H. *Appl. Phys. Lett.* **2011**, *99* (26), 263110.

(13) Carey, C. R.; Yu, Y.; Kuno, M.; Hartland, G. V. *J. Phys. Chem. C* **2009**, *113* (44), 19077−19081.

(14) Lo, S. S.; Major, T. A.; Petchsang, N.; Huang, L.; Kuno, M. K.; Hartland, G. V. *ACS Nano* **2012**, *6* (6), 5274−5282.

(15) Prechtel, L.; Padilla, M.; Erhard, N.; Karl, H.; Abstreiter, G.; Fontcuberta, A.; Morral, I.; Holleitner, A. W. *Nano Lett.* **2012**, *12* (5), 2337−2341.

(16) Prasankumar, R. P.; Upadhya, P. C.; Taylor, A. J. *Phys. Status Solidi B* **2009**, *246* (9), 1973−1995.

(17) Streetman, B. G. *Solid State Electronic Devices*; Prentice Hall: New York, 1995.

(18) Ganikhanov, F.; Burr, K. C.; Hilton, D. J.; Tang, C. L. *Phys. Rev. B* **1999**, *60* (12), 8890−8896.

(19) Allen, J. E.; Hemesath, E. R.; Perea, D. E.; Lensch-Falk, J. L.; LiZ., Y.; Yin, F.; Gass, M. H.; Wang, P.; Bleloch, A. L.; Palmer, R. E.; Lauhon, L. J. *Nat. Nanotechnol.* **2008**, *3* (3), 168−173.

(20) Sabbah, A. J.; Riffe, D. M. *Phys. Rev. B* **2002**, *66* (16), 165217.

(21) Kar, A.; Upadhya, P. C.; Dayeh, S. A.; Picraux, S. T.; Taylor, A. J.; Prasankumar, R. P. *IEEE J. Sel. Top. Quantum Electron.* **2011**, *17*, 889.

(22) Dan, Y.; Seo, K.; Takei, K.; Meza, J. H.; Javey, A.; Crozier, K. B. *Nano Lett.* **2011**, *11* (6), 2527−2532.

(23) Thomsen, C.; Strait, J.; Vardeny, Z.; Maris, H. J.; Tauc, J.; Hauser, J. J. *Phys. Rev. Lett.* **1984**, *53* (10), 989−992.

(24) Mariager, S. O.; Khakhulin, D.; Lemke, H. T.; Kjær, K. S.; Guerin, L.; Nuccio, L.; Sørensen, C. B.; Nielsen, M. M.; Feidenhans'l, R. *Nano Lett.* **2010**, *10* (7), 2461−2465.

(25) Ogi, H.; Shagawa, T.; Nakamura, N.; Hirao, M.; Odaka, H.; Kihara, N. *Phys. Rev. B* **2008**, *78* (13), 134204.

(26) Liss, K. D.; d'Almeida, T.; Kaiser, M.; Hock, R.; Magerl, A.; Eloy, J. F. *J. Appl. Phys.* **2009**, *106* (4), 044914−044916.

(27) Sagar, D. M.; Cooney, R. R.; Sewall, S. L.; Dias, E. A.; Barsan, M. M.; Butler, I. S.; Kambhampati, P. *Phys. Rev. B* **2008**, *77* (23), 235321.

(28) Prasankumar, R. P.; Choi, S.; Trugman, S. A.; Picraux, S. T.; Taylor, A. J. *Nano Lett.* **2008**, *8* (6), 1619−1624.

(29) Hanrath, T.; Korgel, B. A. *J. Phys. Chem. B* **2005**, *109* (12), 5518−5524.

(30) Calarco, R.; Marso, M.; Richter, T.; Aykanat, A. I.; Meijers, R.; v.d. Hart, A.; Stoica, T.; Lüth, H. *Nano Lett.* **2005**, *5* (5), 981−984.

(31) Chin, A. H.; Ahn, T. S.; Li, H.; Vaddiraju, S.; Bardeen, C. J.; Ning, C.-Z.; Sunkara, M. K. *Nano Lett.* **2007**, *7* (3), 626−631.

(32) Edwards, D. F. *Handbook of Optical Constants of Solids*; Academic: New York, 1998.

(33) Jie, J.; Zhang, W.; Peng, K.; Yuan, G.; Lee, C. S.; Lee, S.-T. *Adv. Funct. Mater.* **2008**, *18* (20), 3251−3257.

(34) Duan, X.; Huang, Y.; Cui, Y.; Wang, J.; Lieber, C. M. *Nature* **2001**, *409* (6816), 66−69.